ESCAP/WMO
Typhoon Committee

Available online at www.sciencedirect.com

ScienceDirect

Tropical Cyclone Research and Review 11 (2022) 76–87

www.keaipublishing.com/tcrr

Estimation of mean water vapour residence time during tropical cyclones using a Lagrangian approach

Albenis Pérez-Alarcón [a,b,*], Patricia Coll-Hidalgo [a,c], José C. Fernández-Alvarez [a,b], Raquel Nieto [a], Luis Gimeno [a]

[a] Centro de Investigación Mariña, Universidade de Vigo, Environmental Physics Laboratory (EPhysLab), Ourense, Spain
[b] Departamento de Meteorología, Instituto Superior de Tecnologías y Ciencias Aplicadas, Universidad de La Habana, La Habana, Cuba
[c] Departamento de Meteorología, Empresa Cubana de Navegación Aérea, La Habana, Cuba

Available online 13 August 2022

Abstract

Tropical cyclone (TC)-related rainfall mostly depends on the atmospheric moisture uptake from local and remote sources. In this study, the mean water vapour residence time (MWVRT) was computed for precipitation related to TCs in each basin and on a global scale by applying a Lagrangian moisture source diagnostic method. According to our results, the highest MWVRT was found for the TCs over the South Indian Ocean and South Pacific Ocean basins (~3.08 days), followed by the Western North Pacific Ocean, Central and East North Pacific Ocean, North Indian Ocean, and North Atlantic Ocean basins (which exhibited values of 2.98, 2.94, 2.85, and 2.72 days, respectively). We also found a statistically significant ($p < 0.05$) decrease in MWVRT, at a rate of ~2.4 h/decade in the North Indian Ocean and ~1.0 h/decade in the remaining basins. On average, the MWVRT decreased during the 24 h before TCs made landfall, and the atmospheric parcels precipitated faster after evaporation when TCs moved over land than over the ocean. Further research should focus on the relationship between global warming and MWVRT of atmospheric parcels that precipitate over TC positions.

Keywords: Tropical cyclones; Water vapour residence time; Lagrangian approach; Tropical cyclones precipitation

1. Introduction

Heavy precipitation related to tropical cyclones (TCs), which commonly cause flash flooding, landslide events, and economic and life losses, is one of the most significant impacts of TCs in coastal regions of tropical and subtropical latitudes (Rogers et al., 2009; Willoughby, 2012; Rappaport, 2014). Despite its negative effects, authors have shown the positive role of precipitation associated with TCs in attenuating drought episodes (e.g. Maxwell et al., 2012; Brun and Barros, 2014). Other research findings (Jiang and Zipser, 2010; Xu et al., 2017) have revealed that the contribution of TCs to annual rainfall totals ranged from 3% to 19%. More recently, Guzman and Jiang (2021) found an increasing trend of ~1.3% per year in the average TC rainfall rate.

In general, TC-related precipitation depends on atmospheric moisture availability (Guo et al., 2017; Xu et al., 2017) and moisture transport mechanisms (Schumacher and Galarneau, 2012). Studies have concluded that the moisture transported by these systems is crucial for the water budget over East Asia (Guo et al., 2017) or the North American continent (Xu et al., 2017). More recently, Pérez-Alarcón et al. (2021a, 2022a)

* Corresponding author. Centro de Investigación Mariña, Universidade de Vigo, Environmental Physics Laboratory (EPhysLab), Campus As Lagoas s/n, Ourense, 32004, Spain.
E-mail address: albenis.perez.alarcon@uvigo.es (A. Pérez-Alarcón).
Peer review under responsibility of Shanghai Typhoon Institute of China Meteorological Administration.

Production and hosting by Elsevier on behalf of KeAi

https://doi.org/10.1016/j.tcrr.2022.08.001

measured the origin of moisture for TC-related precipitation during their lifetime along the North Atlantic basin.

Moisture transport mechanisms were strongly modulated by the mean water vapour residence time (MWVRT). This water vapour lifetime is defined as the time that moisture spends in the atmosphere between evaporation and precipitation (Läderach and Sodemann, 2016; Sodemann 2020). Because MWVRT cannot be calculated directly, indirect metrics have been developed to estimate it (Gimeno et al., 2021). One of these indirect metrics is based on the size of the atmospheric reservoir divided by the incoming or outgoing flux (Savenije, 2000); according to this method, MWVRT ranges from 8 to 10 days. Likewise, Trenberth (1998) found a global MWVRT of 8.9 days by applying local depletion times (the rate of water in the atmospheric column and precipitation). Moisture tracking models have been used to estimate it reaching different results. Bosilovich and Schubert (2002) and Yoshimura et al. (2004) have estimated that the MWVRT varies from 7.3 to 9.2 days, a range confirmed as reasonable by Van der Ent and Tuinenburg (2017), who found values of 8–10 days; however, theirs were lower those of Läderach and Sodemann (2016), with an MWVRT of 4–5 days. More recently, Sodemann (2020) concluded that the MWVRT distribution is highly skewed. These discrepancies in MWVRT estimations were mainly caused by the use of different definitions. Gimeno et al. (2021) reconciled these differences by framing MWVRT as a probability density function with a mean of 8–10 days and a median of 4–5 days.

Nevertheless, these studies have generally focused on a global scale and considered the worldwide mechanism of moisture transport and all the weather systems, which have several different lifetimes. This fact was revealed when a particular weather system is analysed separately from the others. For instance, for extratropical cyclones Papritz et al. (2021) found an MWVRT of ~2 days, and for TCs in the North Atlantic Pérez-Alarcón et al. (2022a) showed values from 2.6 to 2.9 days.

Gedzelman et al. (2003) linked the stable isotope ratios of rain and water vapour to the water budget of hurricanes. Based on all the aforementioned evidence, our aim in this study was to estimate the MWVRT for precipitant water vapour during the complete TC lifetime in each oceanic basin of the planet by applying a Lagrangian moisture source diagnostic method. Additionally, an MWVRT interbasin comparison was performed to advance the knowledge of TC climatology.

2. Materials and methods

2.1. Data

The TC historical records (best track archives) over the worldwide oceanic basins were provided by two United States' agencies: the National Hurricane Center (NHC) Atlantic hurricane database (HURDAT2) (Landsea and Franklin, 2013) for the North Atlantic (NATL) and North East Pacific (NEPAC) basins, and the Joint Typhon Warning Center (JTWC) for the remaining basins. Both agencies guarantee the homogeneity of the estimation methods of the TC parameters recorded in the best track records.

The TC size database (TCSize) developed by Pérez-Alarcón et al. (2021b, 2022b) was used to delimit the area inside a TC's outer radius, which is necessary to apply the Lagrangian moisture sources diagnostic method to compute the MWVRT. The study period was set from 1980 to 2018.

The ERA-Interim reanalysis dataset (Dee et al., 2011) from the European Center for Medium Range Weather Forecasting (ECMWF) at 61 vertical levels and 1°×°1 horizontal grid spacing, was used as input data to run the FLEXPART model (Stohl et al., 2005). We used the trajectories of atmospheric parcels from a global FLEXPART experiment, in which the atmosphere was uniformly divided into ~2 million parcels of equal mass every 6 h, which moved with time through a three-dimensional wind field, to determine the moisture sources associated with TC-related precipitation and therefore the MVWRT. Similar experiments with different aims have been performed (Sori et al., 2017; Ciric et al., 2018; Nieto and Gimeno, 2019; Gimeno et al., 2020; Algarra et al., 2020, Pérez-Alarcón et al., 2022a, c).

2.2. Lagrangian MWVRT estimate

To compute the MWVRT of parcels that precipitated over the TC's location (defined by TCSize), we selected those in which the specific humidity decreased more than 0.1 g/kg in the 6 h before arrival at the target area (using the methodology of Läderach and Sodemann (2016)). To identify where air atmospheric parcels gain or lose moisture along their trajectories, we followed them backward in time for up to 10 days by applying the moisture source diagnostic method developed by Sodemann et al. (2008).

An atmospheric parcel can gain or lose a specific humidity (q) along its trajectory through evaporation (e) or precipitation (p), as defined by the Lagrangian water budget equation (Stohl and James, 2004; 2005):

$$(e-p)=\mathrm{m}\left(\frac{\mathrm{dq}}{\mathrm{dt}}\right) \quad (1)$$

where m is the parcel mass. The used of the specific humidity in Eq. (1) allow to estimate the moisture changes in air parcel three dimensionally. The specific humidity change between time t and time $t_{t\text{-}6}$ is assigned to time t according to Eq. (2):

$$\Delta q(t)=q(x(t))-q(x(t-6)) \quad (2)$$

where $x(t)$ denotes the parcel position at time t. Based on the objective selection criteria, a moisture uptake event was identified along a trajectory if a moisture increase occurred ($\Delta q > 0$), but the parcel can also undergo moisture loss ($\Delta q < 0$). Because of the precipitation *en route*, previous moisture uptake from evaporative locations contributed less and less to the precipitation over the target area (Sodemann et al., 2008). Notably, from the end to the start point, the precipitation *en route* was discounted from all previous

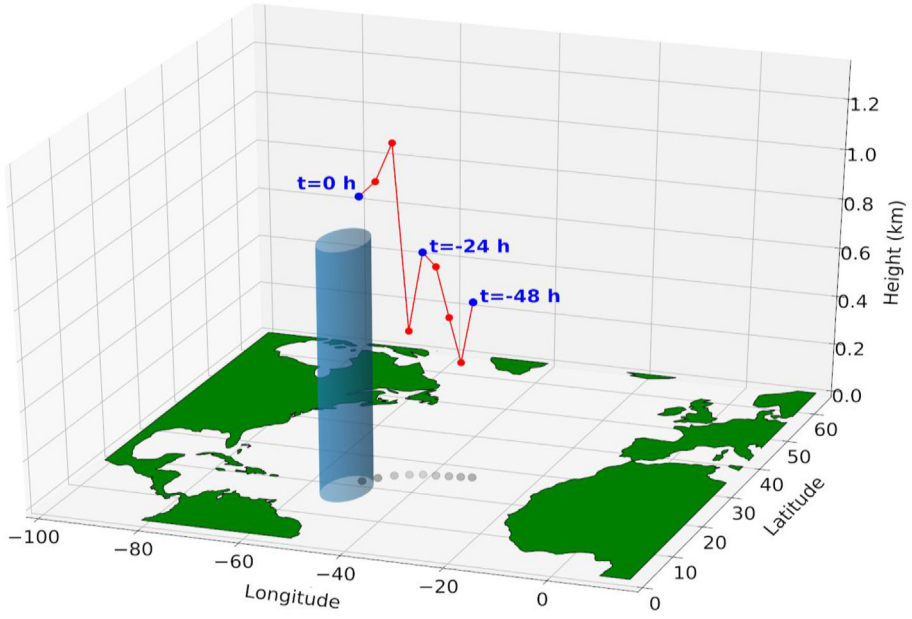

Fig. 1. Three-dimensional schematic representation of the atmospheric particle trajectory of 48 h. Red dots denote the particle position at each time step, grey dots represent the red dot projections over the surface, and the target area is indicated by the blue cylinder.

moisture uptakes in proportion to the precipitation amount, according to Eq. (3):

$$\Delta q_j^{'} = \Delta q_j + \Delta q_i \frac{\Delta q_j}{\sum_{k=t_{end}}^{i-6} \Delta q_k} \quad \text{for all } j > 1 \tag{3}$$

where Δq_i and $\Delta q'_j$ denote the precipitation losses at a precipitation location and the new moisture contribution from previous evaporative locations at times $j > i$, respectively. The fractional contribution (f_c) of each evaporative location at each time step to the final precipitation over the target area can be defined as

$$f_c = \frac{\Delta q'_i}{Q} \tag{4}$$

where Q denotes the moisture content of the atmospheric parcel before its arrival at the target area. Therefore, the water vapour residence time (WVRT) of each parcel was estimated by weighting the effective moisture contribution of each evaporation event to the final precipitation (Läderach and Sodemann, 2016), according to Eq. (5). MWVRT can be computed by averaging the water vapour residence time (WVRT) of all precipitant parcels over the target area.

$$WVRT = \sum_{k=t_{end}}^{t_0} t_k \cdot f_{C_k} \tag{5}$$

Fig. 1 shows a three-dimensional schematic representation of the trajectory of an atmospheric parcel with a length of 48 h. The supplementary information in Läderach and Sodemann (2016) provides a further explanation for this method. As an example, in Fig. 1, we present a detailed description of the

Table 1
Moisture source diagnostic for the particle trajectory in Fig. 1, where *q (g/kg)* is the specific humidity of the atmospheric particle; Δq (g/kg) is the moisture change between sequential time steps, according to Eq. (2); $\Delta q'_j$ (g/kg) is the new moisture contribution of each evaporative location after the discount in proportion the precipitation amount *en route*, according to Eq. (3); and f_c is the fraction of moisture contribution to the final precipitation over the target area.

Time	−48 h	−42 h	−36 h	−30 h	−24 h	−18 h	−12 h	−6 h
q	0.2	4.5	12.1	8.7	10.2	6.4	9.8	12.2
Δq	–	+4.3	+7.6	−3.4	+1.5	−3.8	+3.4	+2.4
$\Delta q'_{-36h}$	–	3.1	5.4	0	–	–	–	–
$\Delta q'_{-24h}$	–	3.1	5.4	0	1.5	–	–	–
$\Delta q'_{-18h}$	–	1.9	3.4	0	0.9	0	–	–
$\Delta q'_{-12h}$	–	1.9	3.4	0	0.9	0	3.4	–
$\Delta q'_{-06h}$	–	1.9	3.4	0	0.9	0	3.4	2.4
f_c	–	0.158	0.283	0	0.075	0	0.283	0.200

WVRT estimation based on the trajectory of a parcel. Table 1 lists the specific humidity values at each time step and their time-step changes. At the starting point of the trajectory, t = −48 h, the atmospheric parcel had a specific humidity value of q = 0.2 g/kg. During the two next time steps, q increases from −48 h to −42 h by +4.3 g/kg, and from −42 h to −36 h by +7.6 g/kg. Subsequently, precipitation occurred *en route* from −36 h to −30 h, losing −3.4 g/kg. According to the aforementioned Läderach and Sodemann (2016) diagnostic method, all previous moisture uptakes (4.3 + 7.6 = 11.9 g/kg) contributed to this precipitation. Therefore, by applying Eq. (3), the new contribution to the final precipitation at t = −42 h was 4.3–3.4 × (4.3/11.9) = 3.1 g/kg. Similarly, for −36 h, 5.4 g/kg was obtained. The parcel again gained +1.5 g/kg from −30 h to −24 h, and lost −3.8 g/kg from −24 h to −18 h. Consequently, the new contribution to the final precipitation at t = −42 h was 3.1–3.8 × (3.1/10) = 1.9 g/kg; at t = −36 h,

3.4 g/kg; and at t = −24 h, 0.9 g/kg. Finally, from −18 h to −12 h and from −12 h to −06 h, the parcel gained 3.4 g/kg and 2.4 g/kg of moisture, respectively.

The last row in Table 1 lists the fractional contributions (Eq. (4)). The WVRT for the final precipitation over the target area was estimated using Eq. (5), resulting in 23.22 h or ~0.97 days.

3. Results and discussion

Fig. 2 reveals notable inter-basin differences in the probability density function (PDF) of TCs trajectories. While TCs over NATL most frequently straight moved toward the Caribbean Sea and the Gulf of Mexico or crossed bordering the north portion of the Antilles islands and the eastern coast of the United States (Fig. 2a), TCs over the NEPAC often described a north-westward track close to the Mexican coast (Fig. 2b). The Bay of Bengal and the Arabian Sea are the home for TCs formed over NIO (Fig. 3c), although they most probably crossed over the former. The PDF of TCs trajectories over SIO exhibited a quasi-zonal maximum in the band between 10°–20°S of latitude and a secondary maximum over the North Australian basin (Fig. 2d), while a zonal pattern was also observed over the Coral Sea in the SPO basin (Fig. 2e). TCs over WNP mainly moved from the western North Pacific to the Philippine Sea and South China Sea (Fig. 2f). Based on the PDFs shown in Fig. 2, TCs in NATL moved over a larger area than in any other basin. Overall, during the study period, WNP recorded approximately 31% of the annual global average of TCs, followed by NEPAC (~20%), SIO (~17%), NATL (~16%), SPO (~11%) and NIO (~5%).

The Lagrangian moisture source diagnostic method for the trajectories of precipitant parcels over the TC locations applied in this study yielded relevant information on the WVRT. Fig. 3 shows the MWVRT for each TC basin. The South Indian Ocean (SIO) and South Pacific Ocean (SPO) basins exhibited the highest MWVRT, with 3.08 ± 0.4 days (uncertainty given as one standard deviation), followed by the Western North Pacific Ocean (WNP) (2.98 ± 0.4 days), NEPAC (2.94 ± 0.4 days), North Indian Ocean (NIO) (2.85 ± 0.4 days), and NATL (2.72 ± 0.4 days). From a global perspective, the MWVRT of atmospheric parcels that became in precipitation over TC locations was estimated to be 2.96 ± 0.4 days.

The MWVRT found in this study is three times lower than the widely used MWVRT of 8–10 days (Trenberth, 1998; Bosilovich and Schubert, 2002; Van der Ent and Tuinenburg, 2017); however, it is closer to, but also lower than, the global estimation of 3.9 ± 0.8 days by Läderach and Sodemann (2016). These studies in the literature were performed for all weather systems on a global scale, not for specific systems such as TCs, as in our case. Additionally, the MWVRT estimate of Läderach and Sodemann (2016) only reported the lifetime of water vapour within the boundary layer. Nevertheless, the circulation associated with evaporating downdraft motion in tropical clouds, and thus in TC clouds (Gray, 2012), transports the colder and drier air from the upper levels to the surface,

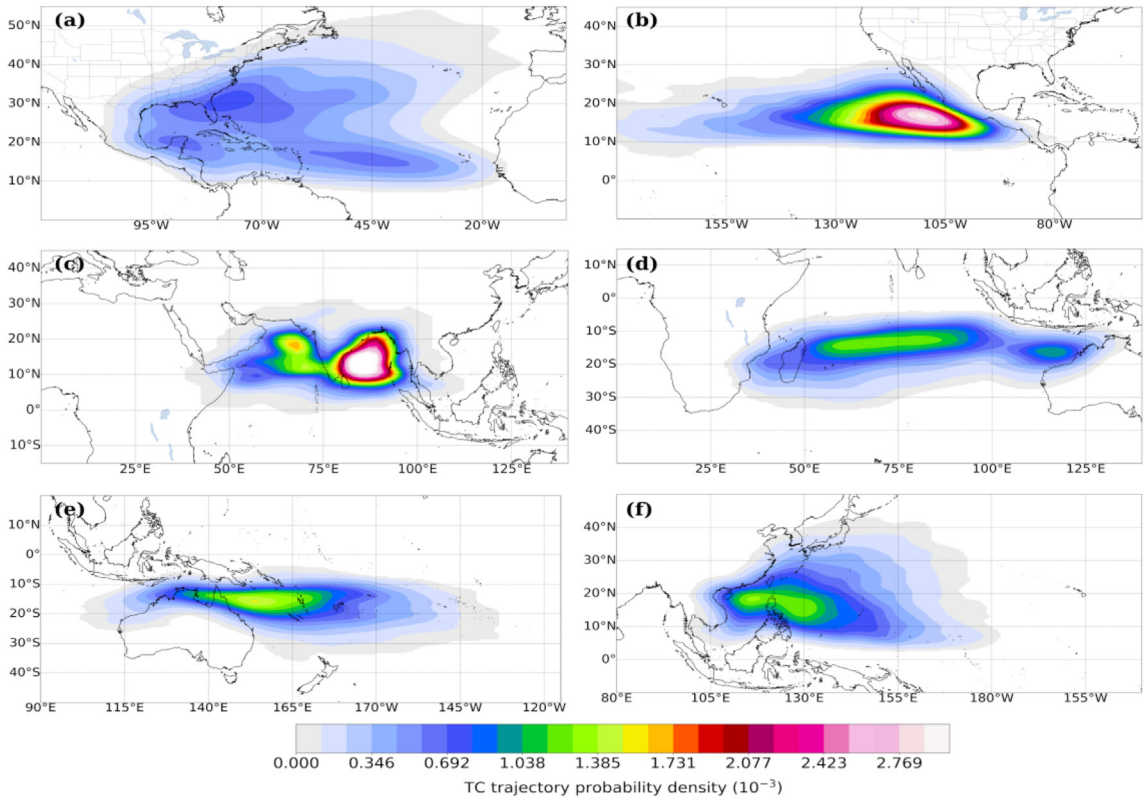

Fig. 2. Probability density of tropical cyclones trajectories over **(a)** North Atlantic Ocean, **(b)** Central and East North Pacific Ocean, **(c)** North Indian Ocean, **(d)** South Indian Ocean, **(e)** South Pacific Ocean, and **(f)** Western North Pacific basins.

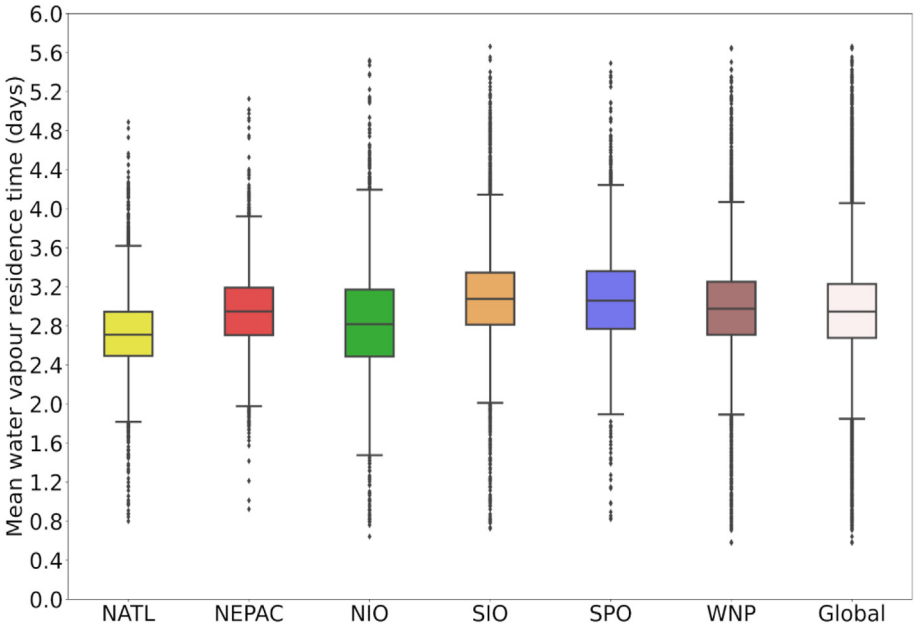

Fig. 3. Lagrangian estimate of mean water vapour residence time. NATL: North Atlantic Ocean, NEPAC: Central and East North Pacific Ocean, NIO: North Indian Ocean, SIO: South Indian Ocean, SPO: South Pacific Ocean, and WNP: Western North Pacific.

leading to a local decrease in MWVRT (Worden et al., 2007; Gimeno et al., 2021), which supports our results.

As the El Niño-Southern Oscillation (ENSO) influences the TC activity in each basin by changes in vertical wind shear, humidity, low-level vorticity, the strength and position of subtropical highs, sea surface temperature (SST) and upper ocean heat content and structure (e.g. Lin et al., 2020), we also computed the MWVRT during the warm (El Niño), cold (La Niña) and neutral phases of ENSO. However, we did not find notable differences in the MWVRT for the precipitation of TCs. Overall, the highest MWVRT values (higher than the mean values in each basin) were found during El Niño, while an opposite pattern was detected during La Niña. Further studies will investigate the influence of climatic modes on the MWVRT during TCs.

Fig. 4 provides a global spatial view of MWVRT for TC-related precipitation. In all basins, the maximum MWVRT values appeared close to the equator, coinciding with the climatological mean position of the Inter-Tropical Convergence Zone (ITCZ, Lashkari et al., 2017; Byrne et al., 2018). This pattern can be directly linked to the upward vertical motion in the ITCZ, which induces generalised moisture convergence from the subtropical regions towards the ITCZ. The higher MWVRTs at low latitudes reflect the quasi-continuous

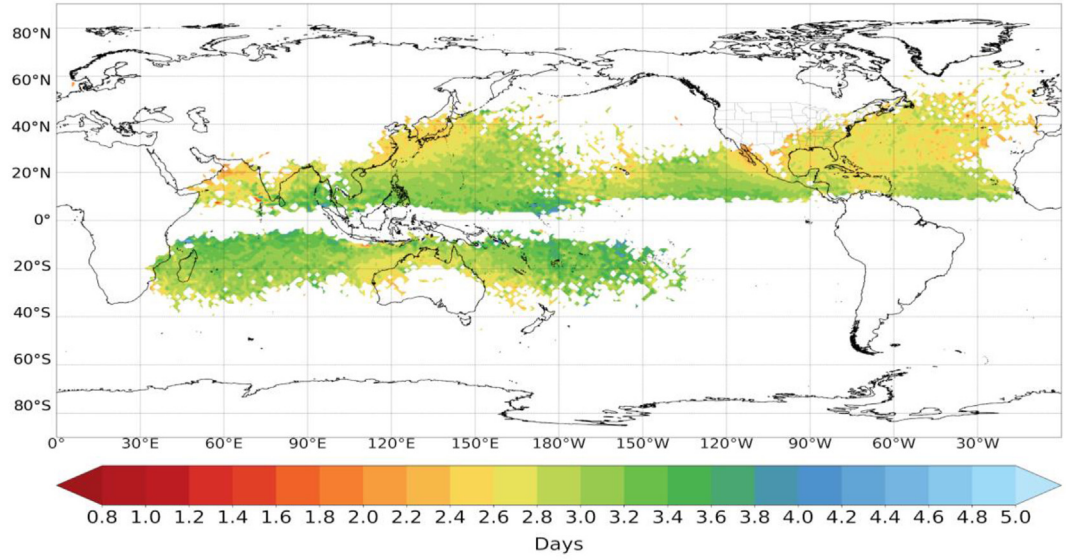

Fig. 4. Mean water vapour residence time (MWVRT) of atmospheric parcels that precipitate over the TC locations from 1980 to 2018. The MWVRT was estimated by applying a Lagrangian moisture source diagnostics method.

evaporation in the subtropics and the subsequent moisture transport driven by the trade winds towards the equator. This result agrees with findings in the literature (Läderach and Sodemann, 2016; Van der Ent and Tuinenburg, 2017; Gimeno et al., 2021).

Fig. 4 also reveals a gradual poleward decrease in MWVRT, which is most evident in the NATL basin. According to Van der Ent and Tuinenburg (2017), regions of low MWVRT coincide mostly with areas of low precipitation. This result can be confirmed by considering that the TC trajectories over the NATL are more dispersed than in the remaining basins (see Fig. 2) and therefore the spatial distribution of TC-related precipitation. The low MWVRT values in the Arabian Sea, Western Caribbean Sea, and surrounding the Gulf of California and the Lower California Peninsula are striking, confirming that regional and local processes influence the spatial distribution of MWVRT, in agreement with Tuinenburg and Van der Ent (2019) and Gimeno et al. (2021).

The spatial distribution of the MWVRT shown in Fig. 4 can also explain why the MWVRT in NIO and NATL show a slightly larger difference than in the remaining basins by comparing it with the global average. In the case of NATL, TCs can move poleward until high latitudes, crossing the subtropics, where the lowest MWVRT values were observed considering only TCs (Fig. 4) or all weather systems (Läderach and Sodemann, 2016; Van der Ent and Tuinenburg, 2017). These lowest values influenced the average time spent by the water vapour in the atmosphere from evaporation to the precipitation over the whole NATL. Conversely, the relatively lower MWVRT values over NIO can be related to the land-sea configuration of NIO, which confines TCs to the Bay of Bengal and the Arabian Sea. The moisture gained by TCs in NIO mainly came from these local sources. Overall, the difference of the average MWVRT in each basin with the global mean could be explained by the heterogeneous distribution of TCs trajectories and evaporation, in agreement with Van der Ent and Tuinenburg (2017).

Several authors (e.g. Bulgin et al., 2020; Pérez-Alarcón et al., 2021c) have addressed the increase in SST in recent decades, and Knutson et al. (2020), using the Clausius–Clapeyron equation, demonstrated that a warmer SST under constant relative humidity conditions favoured higher availability of water vapour. Accordingly, an increase in global MWVRT (considering all weather systems) by 3–6%/ºC has been projected (O'Gorman and Muller, 2010; Gimeno et al., 2021). However, by analysing the annual variation in MWVRT in each basin (Fig. 5), we found a statistically significant decrease ($p < 0.05$) in MWVRT at a rate of ~2.4 h/decade in NIO and ~1 h/decade in the remaining basins. These decreasing trends in the MWVRT of atmospheric parcels that precipitate in TCs could be related to the increasing trend in the average TC rain rate that has been found by Guzman and Jiang (2021) and Tu et al. (2021), caused by the increasing water vapour availability in the atmosphere with rising SST. As aforementioned, a downdraft motion during TC precipitation might decrease MWVRT, in agreement with Gimeno et al. (2021). By computing the Spearman correlation coefficient, while the MWVRT tends to decrease when the amount of precipitation within the TC outer radius increase in NATL and WNP, an opposite pattern was observed in the remaining basins. The correlation coefficients for NATL and WNP, although statistically significant at a 95% confidence level, are too small, being −0.05 and −0.07, respectively. For the other basins, the Spearman correlation coefficients were 0.12, 0.14, 0.24, and

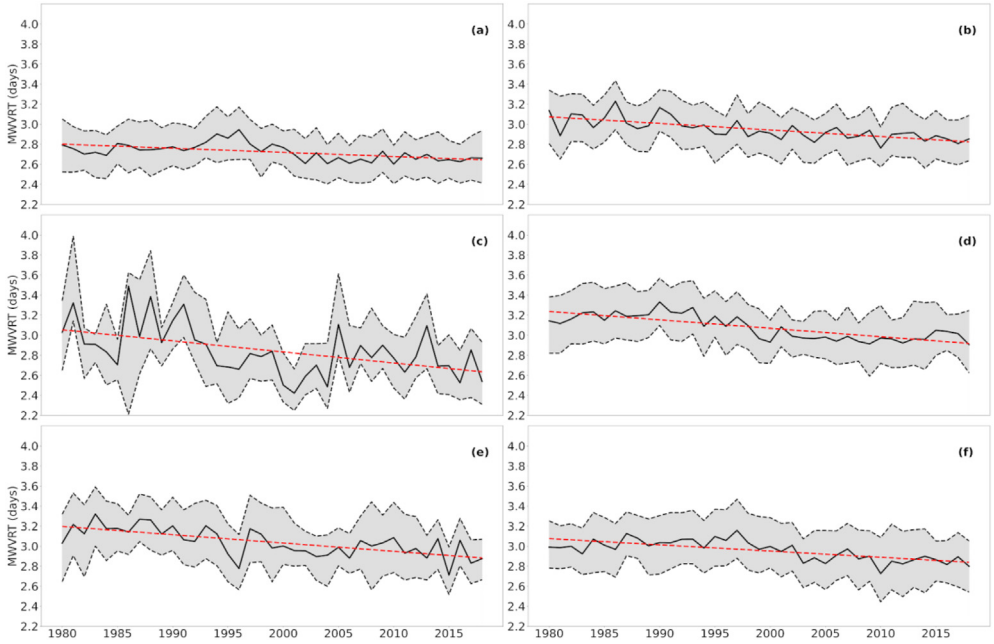

Fig. 5. Annual variation in mean water vapour residence time (MWVRT, solid black line) for precipitation of tropical cyclones in **(a)** North Atlantic Ocean, **(b)** Central and East North Pacific Ocean, **(c)** North Indian Ocean, **(d)** South Indian Ocean, **(e)** South Pacific Ocean, and **(f)** Western North Pacific basins. Red dashed lines represent the statistically significant (at a 95% significance level) trend line; the shaded grey area denotes the interquartile [q1–q3] range.

0.38 for SIO, SPO, NEPAC and NIO, respectively. This relationship is complex due to the several dynamic and thermodynamic processes involved in TCs precipitation. Additionally, the Lagrangian moisture tracking method applied in this work to estimate the MAVRT neglects the presence of liquid water and ice in the atmosphere, evaporation of hydrometeors and mixing of air parcels that can influence the total amount of precipitation (Sodemann et al., 2008).

We also hypothesized that the variability and spread of the MWVRT could be modulated by the same large-scale environmental parameters that modulated TC activity, such as sea surface temperature, 200–850-hPa vertical wind shear, low tropospheric moisture content, 200-hPa divergence and ocean heat content; however, we did not further investigate on how this modulation occurs. Future studies will further explore the variability of the MWVRT for TCs precipitation caused by large-scale environmental factors.

Furthermore, the highest MWVRT occurred in July (the second month of the official TC season) in the NATL basin, but no notable differences were from May to November. The lowest MWVRT was in January and December, but these months are out of the TC season in NATL. For the remaining basins, the monthly MWVRT oscillated around the MWVRT estimated for the study period. Interestingly, we found an MWVRT of ~3.5 days in March for TCs over NEPAC, but it was an atypical value because March is out of TC season, and only one TC formed from 1980 to 2018. These results suggest that the seasonal variation of TCs did not modulate the MWVRT in each basin.

We also found that MWVRT had a significant ($p < 0.05$) inverse Spearman correlation with TC intensity in the SIO (−0.10), NATL (−0.16), NIO (−0.18), WNP (−0.25), and SPO (−0.05), but not in NEPAC. Accordingly, the fastest circulation of air in these basins suggests a short MWVRT, which is expected during the development of intense TCs. Therefore, the discussed decreasing trend in the MWVRT is also supported by the increase in TC intensity over the past four decades (Emanuel, 2005; Elsner et al., 2008; Wing et al., 2007; Holland and Bruyère, 2014; Wang et al., 2017; Bhatia et al., 2019; Kossin et al., 2013; 2020). Nevertheless, this finding must be cautiously interpreted because the sample size was smaller as TCs intensified. For example, the total entries during the H5

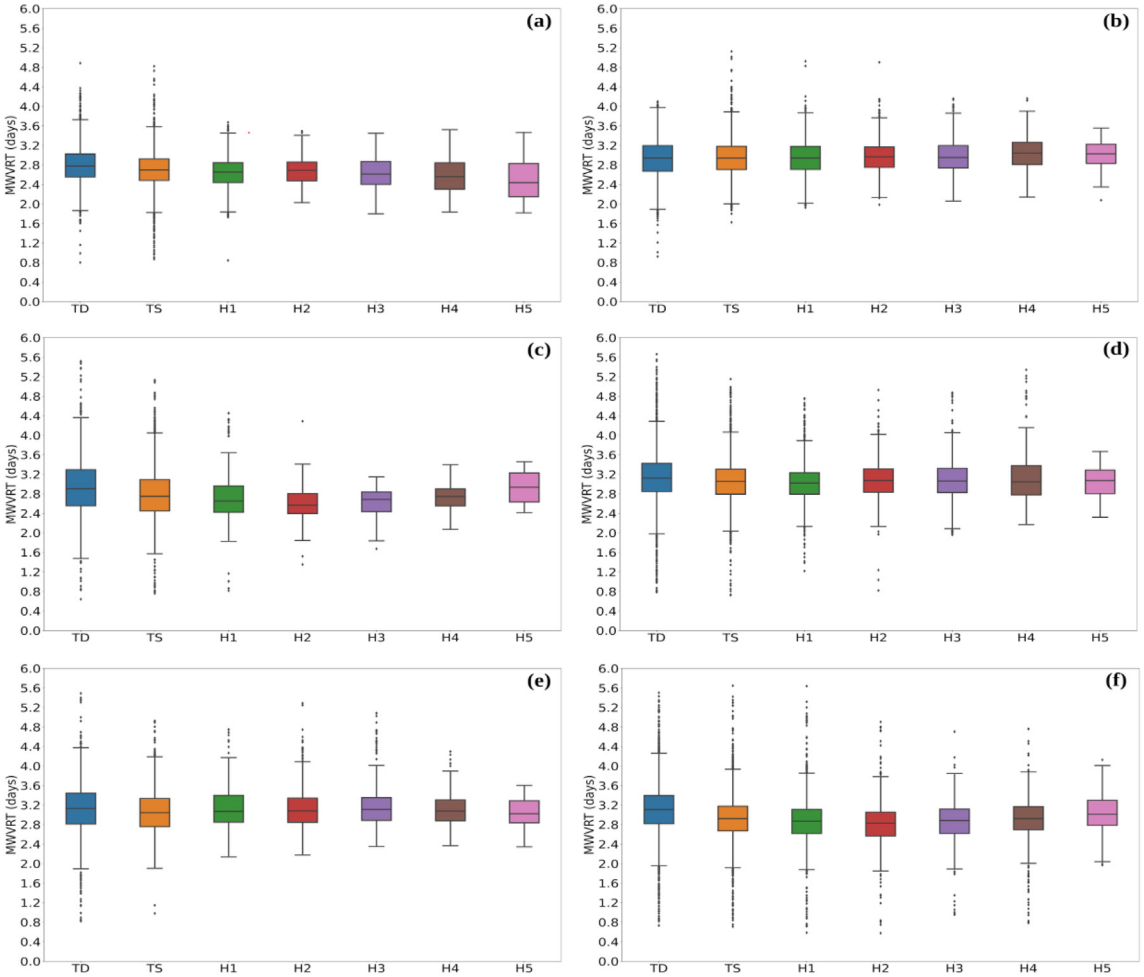

Fig. 6. Lagrangian estimate of mean water vapour residence time for each TC intensity category over **(a)** North Atlantic Ocean, **(b)** Central and East North Pacific Ocean, **(c)** North Indian Ocean, **(d)** South Indian Ocean, **(e)** South Pacific Ocean, and **(f)** Western North Pacific basins. TD: Tropical Depression, TS: Tropical Storm, H_N (N = 1, 2, 3, 4, 5): Hurricane categories on the Saffir-Simpson wind scale.

category represented from 0.2% (in NIO) to 1.2% (in WNP) of all 6-hourly TC records. Therefore, the MWVRT values for stronger TCs could be influenced by the sample size.

These results were partially confirmed by analysing the variations in MWVRT according to intensity categories. Fig. 6a shows a decrease in the MWVRT as TCs intensify in the NATL basin, ranging from ~2.8 ± 0.3 days for tropical depressions (TDs) to ~2.5 ± 0.4 days for Category 5 hurricanes (H5, on the scale Saffir-Simpson wind scale). In the NIO basin, the MWVRT also decreased from ~2.9 ± 0.6 days for TDs to ~2.6 ± 0.3 days for categories H2 and H3 (Fig. 5c). For the WNP, the results were similar to those of NIO, the MWVRT decreased from ~3.1 ± 0.5 days for TDs to ~2.8 ± 0.4 days for category H2, but few differences were found for category H5. In NEPAC, no changes in MWVRT were observed among the categories (Fig. 6b), confirming the weak relationship between TC intensity and MWVRT in this basin. Moreover, the intensity categories in the basins in the Southern Hemisphere did not exhibit significant differences in the MVWRT (Fig. 6d and e), which supported the lower Spearman coefficients between the MWVRT and TC intensity, as discussed in this study. Overall, the highest MWVRT was for TCs in the TD phase (~3.1 ± 0.6 days) and the lowest for category H2 (~2.8 ± 0.4 days).

Pérez-Alarcón et al. (2022c) have shown that remote moisture sources support less atmospheric humidity than those close to the area occupied by TC circulation (our target region), and this phenomenon has a signal in the MWVRT. The MWVRT showed a positive correlation ($p < 0.05$, Spearman test) with the radial distance between the weighted centroid of moisture sources and the boundary of the TCs in the SIO (0.15), NATL (0.22), SPO (0.28), NEPAC (0.35), and WNP (0.35) basins.

3.1. Changes in the Lagrangian MWVRT before TC landfall

Fig. 7a depicts the climatology of the TC tracks 24 h before the landfall. In general, 1320 trajectories were identified and distributed as follows: 79 in NEPAC, 108 in the SPO, 119 in the NIO, 142 in the SIO, 247 in the NATL, and 625 in the WNP. Notably, these values did not represent the total number of landfalling events recorded in each basin during the study period. We only considered landfalling events if the TC moved over the water in the previous 24 h (Rappaport et al., 2010; Liu et al., 2021; Zhu et al., 2021; Fudeyasu et al., 2014).

The MWVRTs in the 24 h before the TC's made landfall were estimated, being ~2.7 ± 0.3 days in the NATL and

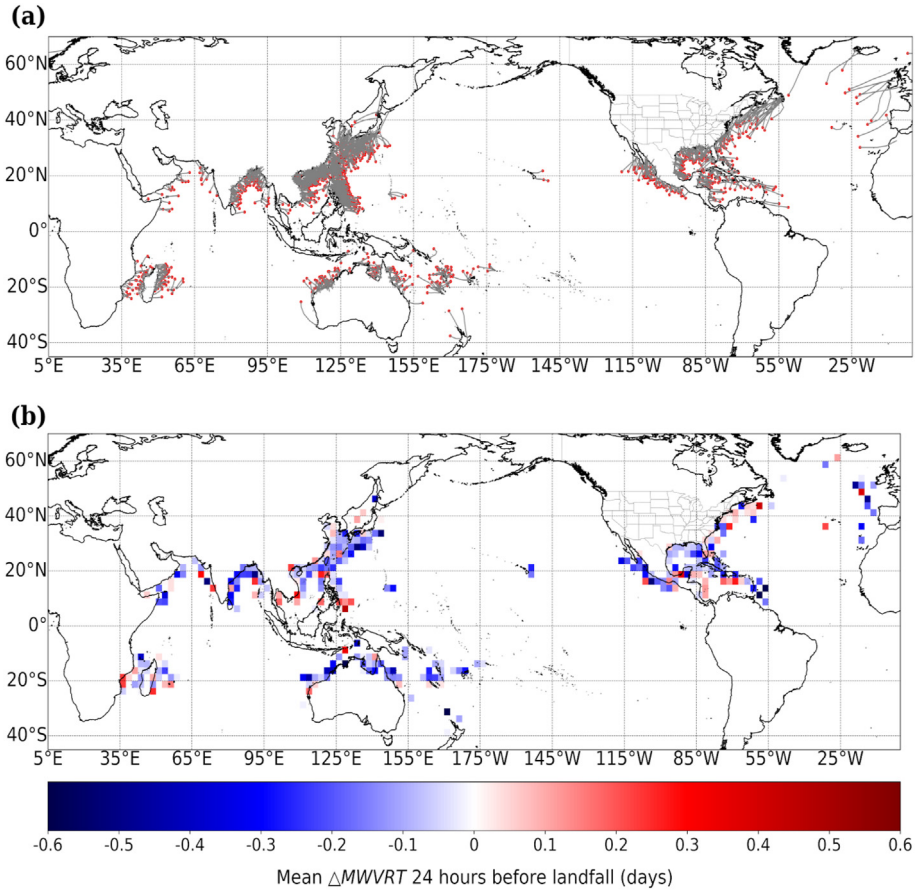

Fig. 7. (a) Tropical cyclone trajectories (grey solid lines) 24 h before landfall from 1980 to 2018 using HURDAT2 databases and Joint Typhon Warning Center best track archives. Red dots indicate the TC position 24 h before landfall. **(b)** Averaged differences of the MWVRT during the 24 h before the TC's landfall, calculated over a 2.5° × 2.5 grid.

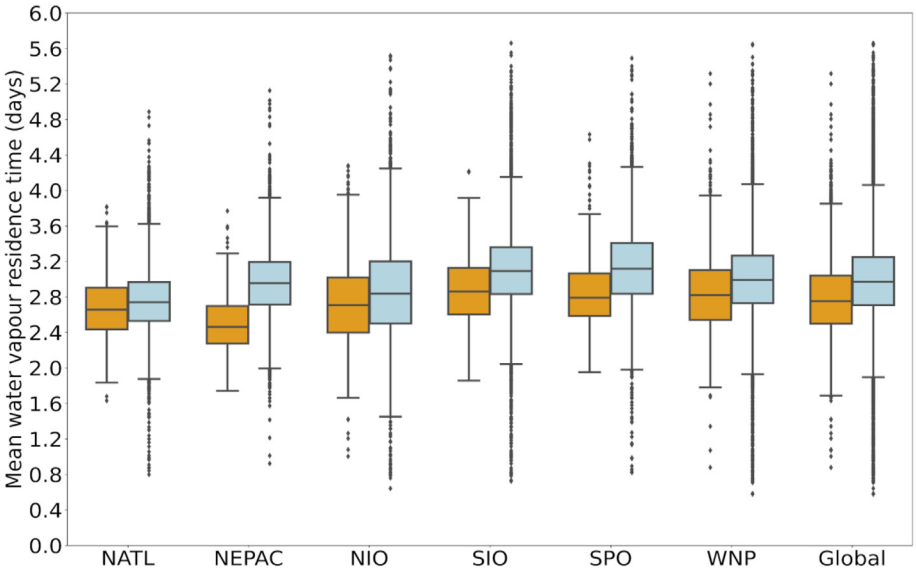

Fig. 8. Lagrangian estimate of mean water vapour residence time when TCs move over ocean (cyan boxes) and over land (orange boxes). NATL: North Atlantic Ocean, NEPAC: Central and East North Pacific Ocean, NIO: North Indian Ocean, SIO: South Indian Ocean, SPO: South Pacific Ocean, WNP: Western North Pacific.

NEPAC, ~2.8 ± 0.4 days in the NIO and WNP, ~2.9 ± 0.4 days in the SIO, and ~3.0 ± 0.4 days in the SPO. Next, we determined if any change occurred along each trajectory: the difference between the MWVRT at landfall and 24 h before landfall was computed, and this value was assigned to the centroid of each 24 h track. Fig. 7b shows these differences averaged over a grid with 2.5 × 2.5 horizontal resolution. Positive (negative) values imply an increase (decrease) in the MVWRT of the atmospheric parcels 24 h before the landfall. In general, a decrease in the MWVRT is observed before a TC's landfall on a global scale, being more notable in the East China Sea, the western Bay of Bengal and the Arabian Sea, the eastern Pacific Ocean bordering the Mexican coast, the seas in northern Australia, and the seas surrounding Cuba, where the values fall between −0.2 and −0.5 days. Likewise, a slight decrease was observed in the Gulf of Mexico, varying from −0.1 to −0.2 days. Fig. 7b also reveals regions where the MWVRT before landfall increases: the Caribbean Sea, the East Coast of the United States, the southern Indochina Peninsula, and the coast of Africa in the Mozambique Channel.

On average, over each ocean basin (Fig. 8), the MWVRT decreased by 3.5% at TC landfall in the NATL basin, and 6.5% and 6.9% in the NIO and SIO, respectively. In the WNP and SPO basins were 9.4% and 9.8%. The reduction in NEPAC is notable: the MWVRT decreased 16.7% at TC landfall. The interaction of TC circulation with land influenced these changes. The general reduction is related to the effects of the orography, which is more evident in mountainous regions than in other areas, inducing changes in the steering flow, and cyclonic circulation tends to favour precipitation processes associated with spiral bands (Lin, 2007; Liu et al., 2016). The high percentage observed in the NEPAC basin may be directly related to the mountainous orography of Central America over TC landfall. Several authors (e.g. Tuleya et al., 1984; Andersen and Shepherd, 2014; Zhu et al., 2021; Wang and Matyas, 2022) have highlighted the impact of the land surface on the dynamics and thermodynamics of TCs, such as the decrease in water vapour availability and low evaporation rate, reducing latent heat flux. During the interaction of the TC circulation with land, the evaporation rate drops dramatically compared with the evaporation rate over the ocean (e.g. Wang and Matyas, 2022), mainly caused by the decreased moisture and increased roughness length over land. Based on these previous findings, we hypothesized that the surface characteristics (e.g. vegetation, orography) influenced the MWVRT after the TCs made landfall.Therefore, studies in more depth than this are required to identify the factors and their linkages with a decrease in MVWRT.

4. Conclusion

The time spent from evaporation to precipitation, or mean water vapour residence time (MWVRT), is a fundamental characteristic of the atmospheric branch of the hydrological cycle. In this study, we applied a Lagrangian moisture source diagnostic method based on backward trajectories up to 10 days from the global outputs of the FLEXPART model to estimate the MWVRT of precipitant parcels during the lifetime of tropical cyclones (TCs) in each ocean basin.

The highest MWVRT was in the South Indian Ocean (SIO) and South Pacific Ocean (SPO) with ~3.08 ± 0.4 days (uncertainty given as one standard deviation). TCs in the North Atlantic basin (NATL) exhibited the lowest value, 2.72 ± 0.4 days. In addition, the MWVRT for the Western North Pacific Ocean (WNP), Central and East Pacific Ocean (NEPAC), and North Indian Ocean (NIO) was estimated to be 2.98 ± 0.4, 2.94 ± 0.4, and 2.85 ± 0.4, respectively. The analysis of all the basins demonstrated that the global MWVRT estimate for TC

precipitation was ~2.96 ± 0.4 days, approximately two–three times lower than the classical estimate of 8–10 days, which considered all weather systems. Nevertheless, the spatial distribution of MWVRT provided a picture that agreed with other global studies, with MWVRT decreasing from the tropics to the subtropics. Therefore, the MWVRT spatial pattern reflected the temporal and spatial scales of moisture transport within the TC location.

Our study also revealed statistically significant decreasing trends in the MWVRT of ~2.4 h/decade in the NIO and a ~1.0 h/decade in the remaining basins, which could be related to the increase in TC intensity and precipitation rates over the last four decades. At global scale, the tropical depressions exhibited the highest MWVRT and Category 2 hurricanes on the Saffir-Simpson wind scale the lowest.

Additionally, we found that the MWVRT generally decreases between 0.2 and 0.5 days in the 24 h before the TCs made landfall, although we identified regions where the MWVRT increased, which was most significant in the Caribbean sea and the east coast of the United States. The MWVRT during this period ranged from 2.7 to 3.0 days. Moreover, the MWVRT decreases over the land by ~3.5% (in NATL) to 16.7% (in NEPAC) of its mean value over the ocean.

This work aimed to advance the knowledge of TC climatology in each basin and on a global scale based on MWVRT. Further research should conduct sensitivity studies to investigate the impact on the MWVRT estimates depending on the length of the backward trajectories and the threshold for considering the occurrence of precipitation. Furthermore, our results lead to new questions regarding how global warming affects the mean residence time of water vapour during TC precipitation. Therefore, further research should analyse the relationship between SST in a warmer climate and the MWVRT of atmospheric parcels that precipitate over TC locations.

Funding

This work was supported by the LAGRIMA and SETESTRELO projects (grants no. RTI2018-095772-B-I00 and PID2021-122314OB-I00, respectively) funded by the Ministerio de Ciencia, Innovación y Universidades, Spain. Partial support was also obtained from the Xunta de Galicia under the Project ED431C2021/44 (Programa de Consolidación e Estructuración de Unidades de Investigación Competitivas (Grupos de Referencia Competitiva) and Consellería de Cultura, Educación e Universidade).

Acknowledgments

A.P-A. acknowledges support from the UVigo PhD grants. J.C.F-A. acknowledges support from the Xunta de Galicia (Galician Regional Government) under grant No. ED481A-2020/193. This work has also been supported by the computing resources and technical support provided by the Centro de Supercomputación de Galicia (CESGA).

Data Availability Statement

The datasets used in this study are freely available on the internet. The ERA-Interim reanalysis dataset was extracted from https://apps.ecmwf.int/datasets/data/interim-full-daily/levtype=sfc/, the HURDAT2 and the JWTC best track archives from https://www.nhc.noaa.gov/data/#hurdat and https://www.metoc.navy.mil/jtwc/jtwc.html?best-tracks. Moreover, the TCSize database was obtain from http://doi.org/10.17632/8997r89fbf.1. The FLEXPART model can be downloaded from https://www.flexpart.eu/wiki/FpRoadmap

References

Algarra, I., Nieto, R., Ramos, A.M., Eiras-Barca, J., Trigo, R.M., Gimeno, L., 2020. Significant increase of global anomalous moisture uptake feeding landfalling Atmospheric Rivers. Nat. Commun. 11, 5082. https://doi.org/10.1038/s41467-020-18876-w.

Andersen, T.K., Shepherd, J.M., 2014. A global spatiotemporal analysis of inland tropical cyclone maintenance or intensification. Int. J. Climatol. 34 (2), 391–402. https://doi.org/10.1002/joc.3693.

Bhatia, K.T., Vecchi, G.A., Knutson, T.R., Murakami, H., Kossin, J., Dixon, K.W., Whitlock, C.E., 2019. Recent increases in tropical cyclone intensification rates. Nat. Commun. 10 (1). https://doi.org/10.1038/s41467-019-08471-z.

Bosilovich, M.G., Schubert, S.D., 2002. Water vapor tracers as diagnostics of the regional hydrologic cycle. J. Hydrometeorol. 3, 149–165. https://doi.org/10.1175/1525-7541(2002)003<0149:WVTADO>2.0.CO;2.

Brun, J., Barros, A.P., 2014. Mapping the role of tropical cyclones on the hydroclimate of the southeast United States: 2002–2011. Int. J. Climatol. 34 (2), 494–517. https://doi.org/10.1002/joc.3703.

Bulgin, C.E., Merchant, C.J., Ferreira, D., 2020. Tendencies, variability and persistence of sea surface temperature anomalies. Sci. Rep. 10, 7986. https://doi.org/10.1038/s41598-020-64785-9.

Byrne, M.P., Pendergrass, A.G., Rapp, A.D., Wodzicki, K.R., 2018. Response of the intertropical convergence zone to climate change: location, width, and strength. Curr. Clim. Change Rep. 4, 355–370. https://doi.org/10.1007/s40641-018-0110-5.

Ciric, D., Nieto, R., Ramos, A.M., Drumond, A., Gimeno, L., 2018. Contribution of moisture from mediterranean sea to extreme precipitation events over danube river basin. Water 10, 1182. https://doi.org/10.3390/w10091182.

Dee, D.P., Uppala, S.M., Simmons, A.J., Berrisford, P., Poli, P., Kobayashi, S., Andrae, U., Balmaseda, M.A., et al., 2011. The ERA-Interim reanalysis: configuration and performance of the data assimilation system. Q. J. R. Meteorol. Soc. 137, 553–597. https://doi.org/10.1002/qj.828.

Elsner, J., Kossin, J., Jagger, T., 2008. The increasing intensity of the strongest tropical cyclones. Nature 455, 92–95. https://doi.org/10.1038/nature07234.

Emanuel, K.A., 2005. Increasing destructiveness of tropical cyclones over the past 30 years. Nature 436, 686–688. https://doi.org/10.1038/nature03906.

Fudeyasu, H., Hirose, S., Yoshioka, H., Kumazawa, R., Yamasaki, S., 2014. A global view of the landfall characteristics of tropical cyclones. Trop. Cyclone Res. Rev. 3 (3), 178–192. https://doi.org/10.6057/2014TCRR03.04.

Gedzelman, S., Lawrence, J., Gamache, J., Black, M., Hindman, E., Black, R., Dunion, J., Willoughby, H., Zhang, X., 2003. Probing hurricanes with stable isotopes of rain and water vapor. Mon. Wea. Rev. 131 (6), 1112–1127. https://doi.org/10.1175/1520-0493(2003)131<1112:PHWSIO>2.0.CO;2.

Gimeno, L., Eiras-Barca, J., Durán-Quesada, A.M., Dominguez, F., van der Ent, R., Sodemann, H., Sánchez-Murillo, M., Nieto, R., Kirchner, J.W., 2021. The residence time of water vapour in the atmosphere. Nat. Rev. Earth Environ. 2 (8), 558–569. https://doi.org/10.1038/s43017-021-00181-9.

Gimeno, L., Nieto, R., Sorí, R., 2020. The growing importance of oceanic moisture sources for continental precipitation. Npj Clim. Atmos. Sci. 3, 27. https://doi.org/10.1038/s41612-020-00133-y.

Gray, W.M., 2012. Fundamental importance of convective downdrafts and mass recycling within the tropical cloud cluster and the typhoon-hurricane. Trop. Cyclone Res. Rev. 1 (1), 130–141. https://doi.org/10.6057/2012TCRR01.14.

Guo, L., Klingaman, N.P., Vidale, P.L., Turner, A.G., Demory, M., Cobb, A., 2017. Contribution of tropical cyclones to atmospheric moisture transport and rainfall over East Asia. J. Clim. 30 (10), 3853–3865. https://doi.org/10.1175/JCLI-D-16-0308.1.

Guzman, O., Jiang, H., 2021. Global increase in tropical cyclone rain rate. Nat. Commun. 12, 5344. https://doi.org/10.1038/s41467-021-25685-2.

Holland, G., Bruyère, C.L., 2014. Recent intense hurricane response to global climate change. Clim. Dyn. 42, 617–627. https://doi.org/10.1007/s00382-013-1713-0.

Jiang, H., Zipser, E.J., 2010. Contribution of tropical cyclones to the global precipitation from eight seasons of TRMM data: regional, seasonal, and interannual variations. J. Clim. 23, 1526–1543. https://doi.org/10.1175/2009JCLI3303.1.

Knutson, T., Camargo, S.J., Chanm, J.C.L., Emanuel, K., Ho, C., Kossin, J., Mohapatra, M., Satoh, M., Sugi, M., Walsh, K., Wu, L., 2020. Tropical cyclones and climate change assessment: Part II: projected response to anthropogenic warming. Bull. Am. Meteorol. Soc. 101 (3), 303–322. https://doi.org/10.1175/BAMS-D-18-0194.1.

Kossin, J.P., Olander, T.L., Knapp, K.R., 2013. Trend analysis with a new global record of tropical cyclone intensity. J. Clim. 26 (24), 9960–9976. https://doi.org/10.1175/JCLI-D-13-00262.1.

Kossin, J.P., Knapp, K.R., Olander, T.L., Velden, C.S., 2020. Global increase in major tropical cyclone exceedance probability over the past four decades. Proc. Natl. Acad. Sci. U.S.A. 117 (22), 11975–11980. https://doi.org/10.1073/pnas.1920849117.

Landsea, C.W., Franklin, J.L., 2013. Atlantic hurricane database uncertainty and presentation of a new database format. Mon. Wea. Rev. 141, 3576–3592. https://doi.org/10.1175/mwr-d-12-00254.1.

Lashkari, H., Mohammadi, Z., Keikhosravi, G., 2017. Annual fluctuations and displacements of inter tropical convergence zone (ITCZ) within the range of Atlantic Ocean-India. Open J. Ecol. 7 (1), 12–33. https://doi.org/10.4236/oje.2017.71002.

Läderach, A., Sodemann, H., 2016. A revised picture of the atmospheric moisture residence time. Geophys. Res. Lett. 43, 924–933. https://doi.org/10.1002/2015GL067449.

Lin, Y.L., 2007. Mesoscale Dynamics, 630. Cambridge University Press, Cambridge. https://doi.org/10.1017/cbo9780511619649.

Lin, I.-I., Camargo, S.J., Patricola, C.M., Boucharel, J., Chand, S., Klotzbach, P., Chan, J.C.L., Wang, B., Chang, P., Li, T., Jin, F.-F., 2020. ENSO and tropical cyclones. In: McPhaden, M.J., Santoso, A., Cai, W. (Eds.), El Niño Southern Oscillation in a Changing Climate. https://doi.org/10.1002/9781119548164.ch17.

Liu, L., Lin, Y.L., Chen, S.H., 2016. Effects of landfall location and approach angle of an idealized tropical cyclone over a long mountain range. Front. Earth Sci 14. https://doi.org/10.3389/feart.2016.00014.

Liu, Q., Song, J., Klotzbach, P., 2021. Trends in western North Pacific tropical cyclone intensity change before landfall. Front. Earth Sci 1025. https://doi.org/10.3389/feart.2021.780353.

Maxwell, J.T., Soulé, P.T., Ortegren, J.T., Knapp, P., 2012. Drought-busting tropical cyclones in the southeastern Atlantic United States: 1950–2008. Ann. Am. Assoc. Geogr. 102 (2), 259–275. https://doi.org/10.1080/00045608.2011.596377.

Nieto, R., Gimeno, L., 2019. A database of optimal integration times for Lagrangian studies of atmospheric moisture sources and sinks. Sci. Data 6, 1–10. https://doi.org/10.1038/s41597-019-0068-8.

O'Gorman, P., Muller, C.J., 2010. How closely do changes in surface and column water vapor follow Clausius–Clapeyron scaling in climate change simulations? Environ. Res. Lett. 5. https://doi.org/10.1088/1748-9326/5/2/025207, 025207.

Papritz, L., Aemisegger, F., Wernli, H., 2021. Sources and transport pathways of precipitating waters in cold-season deep North Atlantic cyclones. J. Atmos. Sci. 78 (10), 3349–3368. https://doi.org/10.1175/JAS-D-21-0105.1.

Pérez-Alarcón, A., Sorí, R., Fernández-Alvarez, J.C., Nieto, R., Gimeno, L., 2021a. Moisture sources for tropical cyclones genesis in the coast of west Africa through a Lagrangian approach. Environ. Sci. Proc. 4, 3. https://doi.org/10.3390/ecas2020-08126.

Pérez-Alarcón, A., Sorí, R., Fernández-Alvarez, J.C., Nieto, R., Gimeno, L., 2021b. Comparative climatology of outer tropical cyclone size using radial wind profiles. Weather Clim. Extrem. 33, 100366. https://doi.org/10.1016/j.wace.2021.100366.

Pérez-Alarcón, A., Fernández-Alvarez, J.C., Sorí, R., Nieto, R., Gimeno, L., 2021c. The relationship of the sea surface temperature and climate variability modes with the North Atlantic tropical cyclones activity. Rev. Cub. Met. 27 (3). http://rcm.insmet.cu/index.php/rcm/article/view/575/1145.

Pérez-Alarcón, A., Sorí, R., Fernández-Alvarez, J.C., Nieto, R., Gimeno, L., 2022a. Where does the moisture for North Atlantic tropical cyclones come from? J. Hydrometeorol. 23 (3), 457–472. https://doi.org/10.1175/JHM-D-21-0117.1.

Pérez-Alarcón, A., Sorí, R., Fernández-Alvarez, J.C., Nieto, R., Gimeno, L., 2022b. Dataset of outer tropical cyclone size from a radial wind profile. Data Br. 40, 107825. https://doi.org/10.1016/j.dib.2022.107825.

Rappaport, E.N., 2014. Fatalities in the United States from Atlantic tropical cyclones: new data and interpretation. Bull. Am. Meteorol. Soc. 95, 341–346. https://doi.org/10.1175/BAMS-D-12-00074.1.

Rappaport, E.N., Franklin, J.L., Schumacher, A.B., DeMaria, M., Shay, L.K., Gibney, E.J., 2010. Tropical cyclone intensity change before US Gulf Coast landfall. Weather Forecast 25 (5), 1380–1396. https://doi.org/10.1175/2010waf2222369.1.

Rogers, R., Marks, F., Marchok, T., 2009. Tropical cyclone rainfall. In: McDonnell, J.J. (Ed.), Encyclopedia of Hydrological Sciences Anderson MG. American Cancer Society. https://doi.org/10.1002/0470848944.hsa030.

Savenije, H.H.G., 2000. Water scarcity indicators; the deception of the numbers. Phys. Chem. Earth B 25, 199–204. https://doi.org/10.1016/S1464-1909(00)00004-6.

Schumacher, R.S., Galarneau, T.J., 2012. Moisture transport into midlatitudes ahead of recurving tropical cyclones and its relevance in two predecessor rain events. Mon. Wea. Rev. 140 (6), 1810–1827. https://doi.org/10.1175/MWR-D-11-00307.1.

Sodemann, H., Schwierz, C., Wernli, H., 2008. Interannual variability of Greenland winter precipitation sources: Lagrangian moisture diagnostic and North Atlantic Oscillation influence. J. Geophys. Res. Atmos. 113, D03107. https://doi.org/10.1029/2007JD008503.

Sodemann, H., 2020. Beyond turnover time: constraining the lifetime distribution of water vapor from simple and complex approaches. J. Atmos. Sci. 77 (2), 413–433. https://doi.org/10.1175/JAS-D-18-0336.1.

Sori, R., Nieto, R., Vicente-Serrano, S.M., Drumond, A., Gimeno, L., 2017. A Lagrangian perspective of the hydrological cycle in the Congo River basin. Earth. Syst. Dyn. 8, 653–675. https://doi.org/10.5194/esd-8-653-2017.

Stohl, A., Forster, C., Frank, A., Seibert, P., Wotawa, G., 2005. Technical Note: the Lagrangian particle dispersion model FLEXPART version 6.2. Atmos. Chem. Phys. 5, 2461–2474. https://doi.org/10.5194/acp-5-2461-2005.

Stohl, A., James, P.A., 2004. Lagrangian analysis of the atmospheric branch of the global water cycle. Part I: method description, validation, and demonstration for the august 2002 flooding in central europe. J. Hydrometeorol. 5, 656–678. https://doi.org/10.1175/1525-7541(2004)005<0656:ALAOTA>2.0.CO;2.

Stohl, A., James, P.A., 2005. A Lagrangian analysis of the atmospheric branch of the global water cycle: Part II: earth's river catchments ocean basins, and moisture transports between them. J. Hydrometeorol. 6, 961–984. https://doi.org/10.1175/JHM470.1.

Trenberth, K.E., 1998. Atmospheric moisture residence times and cycling: implications for rainfall rates and climate change. Clim. Change 39, 667–694. https://doi.org/10.1023/A:1005319109110.

Tu, S., Xu, J., Chan, J.C., Huang, K., Xu, F., Chiu, L.S., 2021. Recent global decrease in the inner-core rain rate of tropical cyclones. Nat. Commun. 12 (1), 1–9. https://doi.org/10.1038/s41467-021-22304-y.

Tuinenburg, O., Van der Ent, R., 2019. Land surface processes create patterns in atmospheric residence time of water. J. Geophys. Res. Atmos. 124, 583–600. https://doi.org/10.1029/2018JD028871.

Tuleya, R.E., Bender, M.A., Kurihara, Y., 1984. A simulation study of the landfall of tropical cyclones. Mon. Wea. Rev. 112 (1), 124–136. https://doi.org/10.1175/1520-0493(1984)112<0124:ASSOTL>2.0.CO;2.

Van der Ent, R.J., Tuinenburg, O.A., 2017. The residence time of water in the atmosphere revisited. Nat. Hazards Earth Syst. Sci. 21, 779–790. https://doi.org/10.5194/hess-21-779-2017.

Wang, C., Wang, X., Weisberg, R.H., Black, M.L., 2017. Variability of tropical cyclone rapid intensification in the North Atlantic and its relationship with climate variations. Clim. Dyn. 49, 3627–3645. https://doi.org/10.1007/s00382-017-3537-9.

Wang, Y., Matyas, C.J., 2022. Simulating the effects of land surface characteristics on planetary boundary layer parameters for a modeled landfalling tropical cyclone. Atmosphere 13 (1), 138. https://doi.org/10.3390/atmos13010138.

Worden, J., Noone, D., Bowman, K., 2007. Importance of rain evaporation and continental convection in the tropical water cycle. Nature 445, 528–532. https://doi.org/10.1038/nature05508.

Willoughby, H.E., 2012. Distributions and trends of death and destruction from hurricanes in the United States, 1900–2008. Nat. Hazards Rev. 13, 57–64. https://doi.org/10.1061/(ASCE)NH.1527-6996.0000046.

Wing, A.A., Sobel, A.H., Camargo, S.J., 2007. Relationship between the potential and actual intensities of tropical cyclones on interannual time scales. Geophys. Res. Lett. 34, L08810. https://doi.org/10.1029/2006GL028581.

Xu, G., Osborn, T.J., Matthews, A.J., 2017. Moisture transport by Atlantic tropical cyclones onto the North American continent. Clim, Dyn. 48, 3161–3182. https://doi.org/10.1007/s00382-016-3257-6.

Yoshimura, K., Oki, T., Ohte, N., Kanae, S., 2004. Colored moisture analysis estimates of variations in 1998 Asian monsoon water sources. J. Meteorol. Soc. Japan 82, 1315–1329. https://doi.org/10.2151/jmsj.2004.1315.

Zhu, Y.J., Collins, J.M., Klotzbach, P.J., 2021. Nearshore hurricane intensity change and post-landfall dissipation along the United States Gulf and East coasts. Geophys. Res. Lett. 48 (17), e2021GL094680. https://doi.org/10.1029/2021gl094680.